Vertically resolved analysis of the Madden-Julian Oscillation highlights the role of convective transport of moist static energy

Da Yang[1], Lin Yao[1], and Walter Hannah[2]

[1]Department of the Geophysical Sciences, University of Chicago
[2]Atmospheric, Earth and Energy Division, Lawrence Livermore National Laboratory

April 26, 2024

Abstract

We simulate the Madden-Julian oscillation (MJO) over an aquaplanet with uniform surface temperature using the multiscale modeling framework (MMF) configuration of the Energy Exascale Earth System Model (E3SM-MMF). The model produces MJO-like features that have a similar spatial structure and propagation behavior to the observed MJO. To explore the processes involved in the propagation and maintenance of these MJO-like features, we perform a vertically resolved moist static energy (MSE) analysis for the MJO. Unlike the column-integrated MSE analysis, our method emphasizes the local production of MSE variance and quantifies how individual physical processes amplify and propagate the MJO's characteristic vertical structure. We find that radiation, convection, and boundary layer processes all contribute to maintaining the MJO, balanced by the large-scale MSE transport. Furthermore, large-scale dynamics, convection, and boundary layer processes all contribute to the propagation of the MJO, while radiation slows the propagation. Additionally, we perform mechanism-denial experiments to examine the role of radiation and associated feedbacks in simulating the MJO. We find that the MJO can still self-emerge and maintain its characteristic structures without radiative feedbacks. This study highlights the role of convective MSE transport in the MJO dynamics, which was overlooked in the column-integrated MSE analysis.

Vertically resolved analysis of the Madden-Julian Oscillation highlights the role of convective transport of moist static energy

Da Yang[1], Lin Yao[1], and Walter Hannah[2]

[1]Department of the Geophysical Sciences, University of Chicago, Chicago, IL, USA
[2]Atmospheric, Earth and Energy Division, Lawrence Livermore National Laboratory, Livermore, CA, USA

Key Points:

- We have successfully simulated the Madden-Julian Oscillation (MJO) using the E3SM-MMF over an aquaplanet with uniform surface temperature.
- Vertically resolved analyses of moist static energy highlight the role of convection in the maintenance and propagation of the MJO.
- Mechanism-denial experiments show that radiative feedbacks are not essential to simulate the MJO.

Corresponding author: Da Yang, dayang@uchicago.edu

Abstract

We simulate the Madden-Julian oscillation (MJO) over an aquaplanet with uniform surface temperature using the multiscale modeling framework (MMF) configuration of the Energy Exascale Earth System Model (E3SM-MMF). The model produces MJO-like features that have a similar spatial structure and propagation behavior to the observed MJO. To explore the processes involved in the propagation and maintenance of these MJO-like features, we perform a vertically resolved moist static energy (MSE) analysis for the MJO (Yao et al., 2022). Unlike the column-integrated MSE analysis, our method emphasizes the local production of MSE variance and quantifies how individual physical processes amplify and propagate the MJO's characteristic vertical structure. We find that radiation, convection, and boundary layer processes all contribute to maintaining the MJO, balanced by the large-scale MSE transport. Furthermore, large-scale dynamics, convection, and boundary layer processes all contribute to the propagation of the MJO, while radiation slows the propagation. Additionally, we perform mechanism-denial experiments to examine the role of radiation and associated feedbacks in simulating the MJO. We find that the MJO can still self-emerge and maintain its characteristic structures without radiative feedbacks. This study highlights the role of convective MSE transport in the MJO dynamics, which was overlooked in the column-integrated MSE analysis.

Plain Language Summary

We conduct simulations of the Madden-Julian oscillation (MJO) using a computer model that can explicitly simulate deep convective clouds. The simulated MJO behaves similarly to what has been observed in the real world in terms of its spatial structure and propagation. We then delve into the detailed mechanisms behind the MJO, using a method that analyzes how energy and moisture move vertically through the atmosphere, rather than just averaging these properties across the whole atmosphere. This novel analysis shows that radiation, convection, turbulence in the atmospheric boundary layer, and large-scale atmospheric flows all play roles in sustaining the MJO and affect its eastward propagation. Interestingly, the MJO can still develop and maintain its unique features without the influence of radiation, indicating other processes are also key. This research underscores the importance of understanding the vertical transport of energy and moisture by convective storms in studying the MJO, an aspect previously underappreciated in some simpler models and diagnoses.

1 Introduction

The Madden-Julian Oscillation (MJO) is a month-long, planetary-scale rainfall pattern in the tropical atmosphere (C. Zhang, 2005). It often initiates in the Indian Ocean and then propagates eastward at about 5 m s^{-1}. This propagation speed is about one third of convectively coupled equatorial Kelvin waves speed and is an order of magnitude smaller than the dry gravity wave speed in the tropical atmosphere. What provides the energy to maintain the planetary-scale circulation and rainfall pattern of the MJO? Why does it propagate eastward? Although the MJO was first discovered in the 1960s, there is still no consensus on the above questions (C. Zhang et al., 2020; Majda & Stechmann, 2009; Adames & Kim, 2016; Yang & Ingersoll, 2013, 2014; Wang et al., 2016). This lack of understanding impeded the progress in simulating the MJO in general circulation models (GCMs) (e.g., Wang et al., 2018).

A popular method to study the MJO is to diagnose its moist static energy (MSE) budget (e.g., Andersen & Kuang, 2012; Pritchard & Yang, 2016; Arnold & Randall, 2015). We define the MSE as $h = c_pT + Lq + gz$, where c_p represents the specific heat capacity of the air at constant pressure, T represents temperature, L represents latent heat of condensation,

q represents specific humidity, g represents gravity acceleration, and z represents altitude. The MSE budget equation is given by

$$\partial_t h' + \nabla_h \cdot (\vec{u}h)' + \partial_p(\omega h)' = Q', \tag{1}$$

where $(\cdot)'$ represents MJO associated quantities, $\vec{u}$ represents horizontal velocity, ω represents pressure velocity, and Q represents sources and sinks of MSE, including radiation, convection, boundary-layer turbulence and other sub-grid scale processes. In particular, Andersen and Kuang (2012) performed vertical integral of this budget, examining the maintenance and eastward propagation mechanisms of MJO-associated MSE anomalies. This analysis framework focuses on horizontal variance of vertically integrated MSE and implicitly assumes that MJO's vertical structure is not fundamental to its dynamics. For example, although Q might have complex vertical structures, it reduces to boundary contributions after the vertical integral. Let's consider the tendency generated by sub-grid scale vertical MSE transport Q_c:

$$\int_{p_s}^{0} Q_c \frac{dp}{g} = -\int_{p_s}^{0} \partial_p F_c \frac{dp}{g} = \frac{F_c|_{p_s} - F_c|_{p=0}}{g} = \frac{F_c|_{p_s}}{g}. \tag{2}$$

Here Q_c can include the effects of convection and boundary layer turbulence, p represents pressure, p_s represents surface pressure, g represents gravity acceleration, F_c represents MSE fluxes, $F_c|_{p_s}$ and $F_c|_{p=0}$ represent the convective MSE fluxes at the surface and top of the atmosphere, respectively. At the upper boundary, convective MSE flux is 0. Then, the vertically integrated contribution due to subgrid-scale vertical MSE transport becomes equivalent to the surface-flux contribution in this framework. This approach simplifies the diagnostic process but also revises the conceptual picture. It may appear that proper surface MSE fluxes would dictate successful MJO simulations regardless of the vertical distribution of convective MSE transport. This could be misleading.

To complement the vertically integrated analysis, we present a vertically resolved MSE analysis to study the MJO. This framework was first developed to study convective self-aggregation (Yao et al., 2022; Yao & Yang, 2023) and was subsequently applied to study tropical cyclones (B. Zhang et al., 2022). The vertically resolved analysis respects the characteristic vertical structure of the MJO and highlights the importance of convective MSE transport to the maintenance and eastward propagation of the MJO. We will present our methods in Section 2, simulation and analysis results in Section 3, and conclusion and discussion in Section 4.

2 The vertically resolved MSE analysis

Our diagnostic framework follows Yao and Yang (2023). The underlying assumption of the analysis is that the MJO has a characteristic vertical structure that is fundamental to the dynamics of the MJO. Then a physical process that has a positive pattern correlation with MJO-associated MSE anomaly $h'(x, y, p)$ increases MJO-associated MSE anomaly, thereby contributing to maintain the MJO. This is analogous to the idea that heating the warm part of the atmosphere increases available potential energy (Lorenz, 1954; Yang, 2018a). We project Equation (1) onto $h'(x, y, p)$ and get the contribution that each term makes to the maintenance of the MJO:

$$\int_{p_T}^{p_S} \frac{dp}{g} \left[\frac{1}{2}\partial_t(\overline{h'^2}) + \overline{h'\nabla_h \cdot (\vec{u}h)'} + \overline{h'\partial_p(\omega h)'} \right] = \int_{p_T}^{p_S} \overline{h'Q'} \frac{dp}{g}, \tag{3}$$

where $\overline{(\cdot)}$ represents horizontal average. Then we normalize Equation (3) by the total MSE variance $\mathcal{A}$ and get the MSE variance budget equation in the unit of growth rate:

$$\text{contribution to growth} = \frac{\text{Equation (3)}}{\mathcal{A}}, \tag{4}$$

where

$$\mathcal{A} = \int_{p_T}^{p_S} \overline{h'^2} \frac{dp}{g}. \tag{5}$$

If the MJO has reached its maintenance stage (*i.e.* statistical equilibrium), $\partial_t h'$ no longer changes the overall amplitude of the MJO but instead describes the propagation of the MJO. Therefore, to assess the contribution of each term to this propagation, we project Equation (1) onto $\partial_t h'$:

$$\text{contribution to propagation} = \frac{\int_{p_T}^{p_S} \overline{\partial_t h' \cdot S} dp/g}{\mathcal{B}}, \tag{6}$$

where S represents a given term in Equation (1), and

$$\mathcal{B} = \int_{p_T}^{p_S} \overline{(\partial_t h')^2} \frac{dp}{g}. \tag{7}$$

In contrast to the vertically integrated analysis, our approach first calculates the spatial MSE variance and then performs the vertical integral. This subtle change in the operation order allows us to objectively diagnose if the vertical distribution of MSE fluxes, e.g., via convection, makes a significant contribution to the MJO's maintenance and propagation.

To the best of our knowledge, there are two major studies that have presented analysis results explicitly resolving the vertical dimension. Chikira (2014) noticed the limitations of the vertically integrated framework and performed a detailed budget analysis of the specific humidity anomalies associated with MJO, in a spirit similar to our study. However, the author did not quantify the contribution of each process to the development, maintenance, and propagation of the MJO. Wolding et al. (2016) assumed a weak horizontal temperature gradient and developed a vertically resolved analysis method for the MJO. That framework may work well in the free troposphere but does not apply to the boundary layer, where a substantial horizontal temperature gradient can be sustained.

3 Methods

3.1 Model Description

E3SM was originally forked from the NCAR CESM (Hurrell et al., 2013), but all model components have undergone significant development since then (Golaz et al., 2019; Xie et al., 2018). The dynamical core uses a spectral element method on a cubed-sphere geometry (Ronchi et al., 1996; Taylor et al., 2007). Physics calculations, including the embedded cloud-resolving models (CRMs) in E3SM-MMF, are performed on a finite volume grid that is slightly coarser than the dynamics grid, but more closely matches the effective resolution of the dynamics (Hannah et al., 2021).

The multi-scale modelling framework (MMF) configuration of E3SM (E3SM-MMF) was originally adapted from the super-parameterized CAM (SP-CAM; Khairoutdinov et al., 2005). E3SM-MMF has also undergone significant development, but still reproduces the general behavior of its predecessor (Hannah et al., 2020). The embedded CRM in E3SM-MMF is adapted from the System for Atmospheric Modeling (SAM) (Khairoutdinov & Randall, 2003), but rewritten in C++ using the performance portability library of Yet

Another Kernel Launcher (YAKL) [1] to facilitate GPU hard acceleration. Microphysical processes are parameterized with a single moment scheme, and sub-grid scale turbulent fluxes within the CRM are parameterized using a diagnostic Smagorinsky-type closure. There is an additional boundary layer scheme outside of the CRM based on Holtslag and Boville (1993). This allows surface momentum fluxes to be mixed through the boundary layer prior to calling the global dynamics, which reduces a problematic near-surface wind bias. Aerosol and ozone concentrations are prescribed with present-day values.

E3SM-MMF uses a 60 layer vertical grid with 50 levels in the embedded CRM. The embedded CRM in E3SM-MMF uses a two-dimensional domain with 64 CRM columns in a north-south orientation and 2 km horizontal grid spacing. The global physics time step is set at 20 minutes with a CRM time step of 10 seconds. The CRM variance transport scheme of Hannah and Pressel (2022) is enabled to reduce grid-scale noise caused by variance trapping in the CRM (Hannah et al., 2022).

3.2 Model Simulations

The model was configured for radiative-convective equilibrium (RCE) according to the RCE model intercomparison project protocol (Wing et al., 2018). This includes globally homogeneous surface temperature of 300K and globally homogeneous downward shortwave radiation. Additionally, rotation was enabled to create an equatorial wave guide. This global RCE setup is a further simplification from aquaplanet simulations with meridional surface temperature gradient and avoids interference from middle latitude weather systems (e.g., Hu et al., 2008). The simulations were run for 9 years using 128 nodes of the NERSC Perlmutter. The standard global cube-sphere grid was used with 30x30 spectral elements per cube face and 2x2 FV physics cells per element (i.e. ne30pg2), with a physics grid spacing of 150 km.

To explore the role of cloud-radiative feedbacks in the MJO-like phenomena that emerge in these simulations we use two methods for spatially homogenizing the radiative tendencies. In the first method, abbreviated as "HomoRad", we allow radiation to be calculated in every column at each global model physics step, but before tendencies can be applied to the state, we calculate a global average at each model level that is then applied to each column. This method allows the global equilibrium to adjust in time. In the second method, abbreviated as "FixedRad", we use fixed profiles of longwave and shortwave radiative heating tendencies calculated as the global and temporal averaged profiles from the control run, which are then applied to the state instead of calling the radiation scheme.

4 Results

E3SM-MMF can successfully simulate the MJO over an aquaplanet with a uniform SST. Figure 1a plots anomalous outgoing longwave radiation (OLR) of our control simulation. There are small-scale, short-lived waves that propagate both eastward and westward. In addition, there are wave envelops that span about half of the equatorial circumference and can last longer than 50 days. These large-scale signals are the MJOs and propagate eastward at about 9 m/s. We then perform a 2D Fourier transform of the OLR anomaly and plot its power spectrum (Fig. 2a), where the MJO stands out as the most dominant intraseasonal variability as in observations.

We construct the MJO composites following Ma and Kuang (2011). To detect convective centers, we first average the daily OLR data across the latitudinal range of 10°S to 10°N. Then, we filter the meridionally averaged OLR within the MJO's spectral window, targeting zonal wavenumbers 1 to 9 and periods from 20 to 100 days (Fig. 2a), using the

[1] see `https://github.com/mrnorman/YAKL` for more information

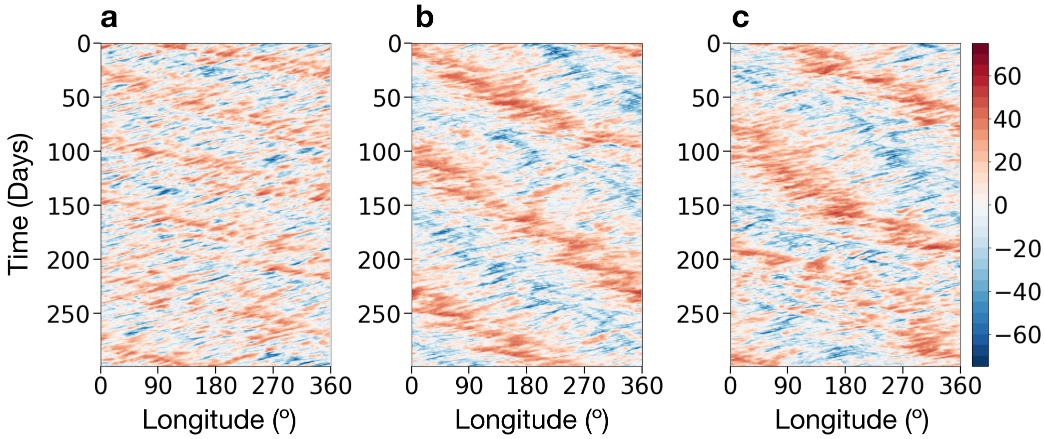

Figure 1. Hovmoller diagrams of OLR anomalies in (a) the control simulation, (b) the HomoRad simulation, and (c) the FixedRad simulation.

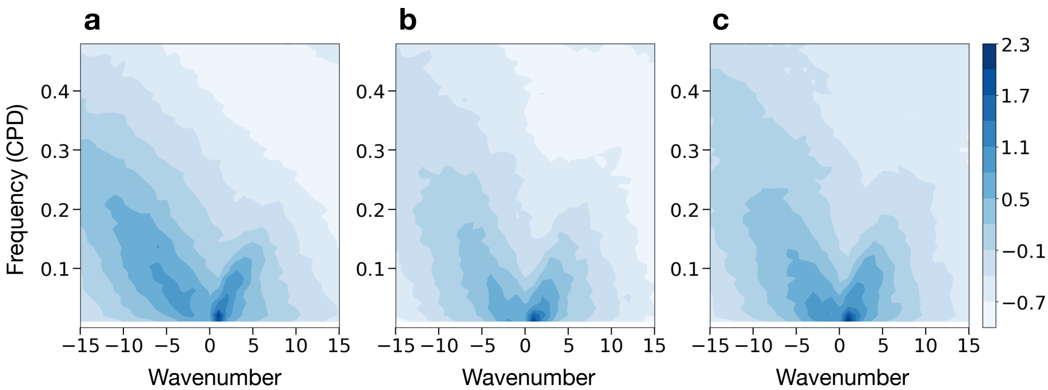

Figure 2. The power spectra of OLR in (a) the control simulation, (b) the HomoRad simulation, and (c) the FixedRad simulation.

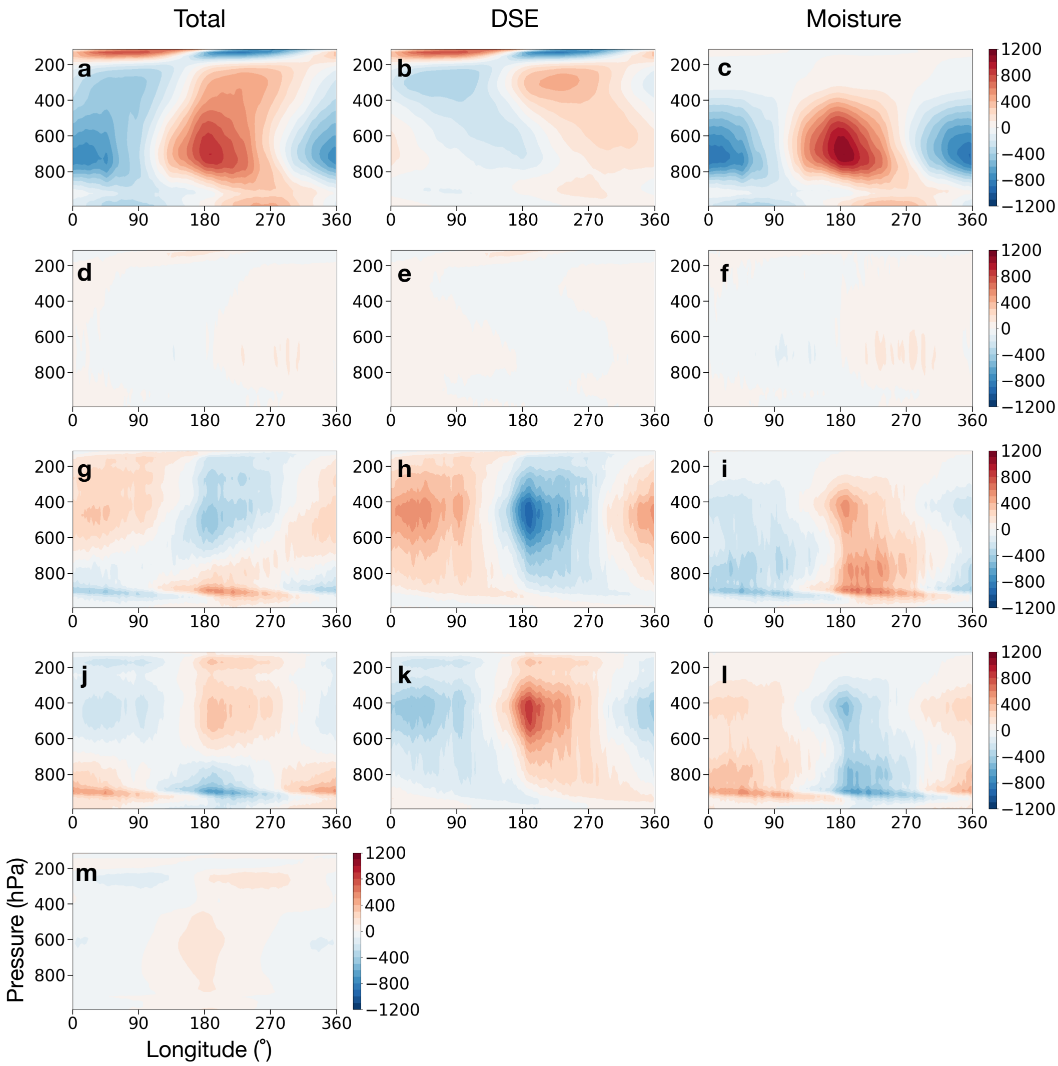

Figure 3. Vertical structures of the MSE budget of the MJO composite. The first column presents terms in Equation (1). Then we decompose these terms into components associated with dry static energy and specific humidity and plot them in the second and third columns. The first row represents MJO's MSE anomalies (units: J/kg). The second row represents total MSE tendency ∂_tMSE (units: J/kg/day). The third row represents the effect of large-scale dynamics in transporting and redistributing MSE. The fourth row represents the effect of CRM and boundary layer schemes in transporting and redistributing MSE. The last row represents the effect of radiation. Although convection does not change column-integrated MSE, it does redistribute MSE within a given column and thus changes local MSE.

method of Wheeler and Kiladis (1999). Thereafter, the lowest OLR value is identified as the convective center on each day. In creating the MJO composites, we calculate anomalies by subtracting zonal averages. Subsequently, we rearrange the data on each day to ensure that each convective center is strategically placed at 180°, which is the center longitude of the maps. Finally, we average the rearranged data over time to produce the composites. For 3D variables in the MSE budget equation, we further average the variables across the same latitudinal span (10°S to 10°N) to illustrate the characteristic vertical structures.

Figure S1a plots the composite OLR and 200-hPa geopotential anomalies of the MJO. The horizontal structure of the simulated MJO is similar to the observations and model simulations (Andersen & Kuang, 2012; Arnold & Randall, 2015; Straub & Haertel, 2005). Both the OLR and geopotential anomalies are symmetric about the equator and with peaks right at the equator. Negative OLR anomalies correspond to the convective regions of the MJO, spanning over 150^o longitudes and 30^o latitudes. The geopotential anomalies show distinct quadrupole structures, which is often interpreted as a Gill-type response (Gill, 1980) to a pair of heating and cooling anomalies on the equator, associated with MJO's enhanced and suppressed convection, respectively.

We apply the same compositing technique to analyze the MJO-associated MSE anomalies (Fig. 3a). In this process, we rearrange the data so that the convective center of the MJO is at 180^o longitude. There are large-scale ascending motions near the convective center and descending motions elsewhere. The composite MSE anomalies show a peak in the lower troposphere, around 650 hPa. Above this level, the MSE anomalies tilt eastward; below this level, the MSE anomalies tilt westward. Such a distinct vertical structure looks similar to what we observe in the real tropical atmosphere and may result from a combination of the first, second, and potentially higher vertical modes (Andersen & Kuang, 2012; Haertel et al., 2008; Straub & Haertel, 2005). We further decompose the MSE anomalies into the dry static energy component (DSE $= c_pT + gz$) and the moisture component (Lq). The DSE component (Fig. 3b) is generally weaker than the moisture component (Fig. 3c), except for the upper troposphere. That may result from the weak buoyancy gradient nature of the tropical atmosphere. There, the Rossby number is large, and the Froude number is small. That leads to a small horizontal buoyancy gradient (Charney, 1963; Yang & Seidel, 2020; Yang, 2018b; Seidel & Yang, 2020; Yang et al., 2022). Therefore, the vertical structure of the MSE anomalies mainly follows that of the moisture component.

The rest of Figure 3 detail composites of individual terms from the MSE budget equation (Equation 1), using a uniform color scale across all panels to ease the comparison of their magnitudes. Figure 3d-f shows the MSE tendency $\partial_t h'$ and its DSE (∂_tDSE) and moisture ($\partial_t Lq$) components. The magnitude is weak, and the signal leads the MSE anomaly by a quarter cycle. This result indicates that the MJO would maintain its amplitude while propagating eastward. Thus $\partial_t h'$ does not project strongly onto the MSE anomaly but instead is responsible for the eastward propagation of the MJO.

Figure 3g shows the large-scale MSE convergence $-\nabla_{3D} \cdot (\vec{u}h)'$, where $(\vec{u}h)'$ represents MSE flux due to large-scale circulations. Near the convective center, $-\nabla_{3D} \cdot (\vec{u}h)'$ is positive in the lower troposphere, suggesting an up-gradient MSE transport; $-\nabla_{3D} \cdot (\vec{u}h)'$ becomes negative in the upper troposphere due to large-scale winds exporting MSE to the subsiding regions. To understand this rich vertical structure, we decompose $-\nabla_{3D} \cdot (\vec{u}h)'$ into DSE and moisture components, both of which have simpler vertical structures (Fig. 3h-i). Large-scale ascending motions are present over the convective regions, and they adiabatically cool (Fig. 3h) and moisten (Fig. 3i) the atmosphere throughout the depth of the troposphere, except for the near-surface levels to the west of the convective center. Meanwhile, large-scale descending motions are present and adibatically warm and dry the atmosphere over clear-sky regions. Therefore, the competing effects of the DSE and moisture components lead to the complex vertical structure in Fig. 3g. Adiabatic cooling (and warming) proves more significant in the upper troposphere, whereas moistening (and drying) predominantly affects the lower troposphere.

In E3SM-MMF, the vertical MSE transports by convection and boundary layer turbulence are treated separately, but their effects are similar–redistributing MSE without changing the column-integrated MSE. Therefore, we consider them as an integral part and present their MSE transports together (Fig. 3j). As shown in Eqn. (2), convergence of convective MSE flux yields a positive local MSE tendency, and divergence of convective MSE flux yields a negative local MSE tendency. The overall effect is to stabilize the air column by transporting high MSE air from the boundary layer to the free troposphere. This transport of MSE is associated with convective heating that increases DSE (Fig. 3k) and condensation that decreases specific humidity (Fig. 3l). Their net effect reduces (increases) MSE in the lower (upper) troposphere over the convective regions.

There appears to be a significant compensation between the convective MSE transport and large-scale MSE convergence when we compare the third and fourth rows of Fig. 3. This compensation was discussed in detail by Emanuel et al. (1994). Large-scale flows converge high-MSE air in the boundary layer toward the convective center. Then, small-scale turbulence and convection transport the high-MSE air to the free troposphere, where the large-scale circulation exports it to surrounding areas. As we will discuss, the net effect of the large-scale and the small-scale parameterized dynamics tends to stabilize the circulation.

To further understand the collective effects of convection and large-scale circulations, we add the third and fourth rows of Fig. 3 together and get Fig. S2. We reproduce MJO's MSE anomaly and its total tendency (∂_tMSE) in Fig. S2 a & b for convenience. Fig. S2 c shows the MSE tendency due to convection and circulations, which has a spatial pattern very similar to that in Fig. S2 b, confirming that convection and circulations are responsible for MJO's eastward propagation. We then decompose Fig. S2 c into DSE and moisture components shown in Fig. S2 d & e, respectively. Their contribution to the DSE tendency is largely out of phase with the MSE anomaly in Fig. S2 a, suggesting a damping or stabilizing effect. Their contribution to the moisture tendency leads the MSE anomaly by a quarter cycle and is in phase with ∂_tMSE, suggesting that the moisture component is mainly responsible for the propagation.

To put this result into context, we assume that the MJO's MSE anomaly h' has the form of a propagating wave:

$$h' = \hat{h} e^{ikx+\sigma t},$$

where $\hat{h}$ represents MJO's amplitude, k and σ represent zonal wavenumber and growth rate respectively. Our diagnosis suggests that convection and circulation's contribution to the DSE tendency is associated with the real part of σ, and their contribution to moisture is associated with the imaginary part.

Radiative heating anomalies appear largely in phase with the MSE anomalies, suggesting a positive contribution to maintaining the MJO (Fig. 3m). Over the convective regions, there is anomalous water vapor and cloud cover leading to positive radiative heating anomalies that further support upward motions and convection. This forms a positive feedback loop between water vapor, clouds, and radiation. Over the dry subsiding regions, radiation effectively cools the atmosphere and induces subsidence. The amplitude of radiative heating anomalies is weak but consistent with pressure levels over the convective region. This particular vertical structure makes radiative heating anomaly project strongly onto the MJO's MSE anomaly.

We conduct a quantitative analysis of each term's role in sustaining the MJO by plotting Equation (4) in Figure 4a. Radiation is identified as the primary factor in the MJO's maintenance, aligning with previous findings from column-integrated analyses (Andersen & Kuang, 2012; Arnold & Randall, 2015; Pritchard & Yang, 2016). Additionally, the net influence of convection is significant, but its effects on DSE and moisture are opposite. For example, over the convective areas, drying effects through condensation and precipitation decrease MSE, while convective heating increases MSE. Large-scale flows tend to reduce the

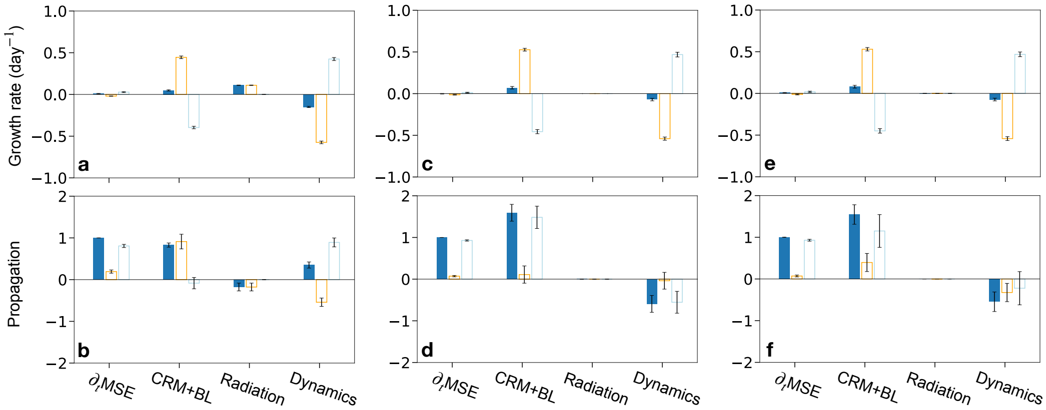

Figure 4. The MSE budget for the control simulation (first column), HomoRad simulation (second column), and FixedRad simulation (third column). The first and second rows show individual terms' contribution to MJO's maintenance and propagation, respectively. The solid blue bar represents MSE; the open orange and blue bars represent the corresponding DSE and moisture components, respectively. In the second and third columns, the radiative heating rate is horizontally uniform, so it does not contribute to maintaining and propagating MSE anomalies.

MJO amplitude mainly through adiabatically cooling the area with positive MSE anomalies. Again, the effects of convection and large-scale flows compensate significantly in maintaining the MJO.

We then assess each term's contribution to MJO's eastward propagation by plotting Equation (6) in Fig. 4b. Convection is primarily responsible for the eastward propagation of the MJO, predominantly through its heating, not its associated drying effect due to condensation. Radiation slightly hinders the eastward progression. On the other hand, large-scale dynamics support the eastward propagation, where adiabatic cooling retards the eastward propagation, and moistening effects favor the eastward propagation.

5 Mechanism-denial experiments

Although radiation is a major factor in maintaining the MJO, our diagnostic results show that convection's contribution is of the same order of magnitude (Fig. 4a). This result motivates mechanism-denial experiments to examine if interactive radiation or radiative feedbacks are essential to the MJO. We perform two experiments, in which we horizontally homogenize the radiative heating rate and prescribe a uniform radiative heating rate, respectively (Section 3c). Both methods can effectively decouple radiation from MJO's thermodynamic and circulation patterns, switching off a positive feedback. However, E3SM-MMF can still simulate MJOs without the radiative feedback (Figs. 1, 2), and they show horizontal structures similar to those in the control simulation (Fig. S1). Although the simulation results disagree with the global 20-km resolution simulations by Khairoutdinov and Emanuel (2018), our results agree well with superparameterized GCM results in Arnold and Randall (2015) and Grabowski (2003). Through our vertically resolved MSE analyses, we find that convective MSE transport is sufficient to maintain the MJO (Fig. 4c, d).

It would be intuitive to assume that the MJO becomes weaker in the mechanism-denial experiments. However, the MJO's OLR anomalies seem to become stronger, while wind anomalies (e.g., Rossby wave gyres) become weaker (Figs. 1, S1). This result may suggest that the maintenance of MJO involves nonlinear processes, and understanding this counter-intuitive result may require a finite-amplitude theory that goes beyond linear analysis.

6 Conclusion and Discussion

This paper presents MJO simulations over an aquaplanet with a uniform surface temperature using E3SM-MMF. The simulated MJOs have similar spatial structures and propagation behavior to observations. We consider that the MJO has a characteristic vertical structure that is fundamental to its dynamics. Therefore, to understand the propagation and maintenance of the MJO, we perform a vertically resolved MSE analysis for the MJO (Yao et al., 2022). Our method quantifies how individual physical processes amplify and propagate the characteristic vertical structure of the MJO. Our analyses show that both radiation and convection (CRM + boundary layer) contribute to maintaining the MJO, balanced by the large-scale dynamic transport of MSE. Furthermore, convection is primarily responsible for the eastward propagation of the MJO, while radiation may slightly retard the propagation. The diagnostic results seem to suggest that the MJO can still develop and maintain even without interactive radiation and associated feedbacks. This hypothesis is then confirmed by mechanism-denial experiments.

Although convection does not change the column-integrated MSE, convection can indeed change local MSE. Our diagnostic analysis and mechanism-denial experiments highlight the role of convection in both MJO's maintenance and propagation. This result may appear to agree with a school of studies proposing that convection drives MJO (Yang & Ingersoll, 2013, 2014; Wang & Chen, 1989; Wang & Rui, 1990; Majda & Stechmann, 2009). However, in the column integrated analysis, such vertical MSE transport reduces to boundary contributions, and thus, the effects would be overlooked by design (see Eq. 2). It's important to note that several moisture-mode models for the MJO (e.g., Adames & Kim, 2016; Ahmed, 2021) predominantly use vertically integrated equations for temperature, moisture, or MSE. This approach may inadvertently fail to capture the complete effects of convection on the MJO's maintenance and propagation, suggesting a potential area for improvements in these models.

Why does super-parameterization of convection lead to better MJO simulations? What does traditional convection parameterization lack in simulating the MJO? These questions have puzzled our field for more than a decade. Our analysis method can help diagnose GCM simulations and address the above questions. We plan to perform E3SM simulations using the same model setup and conduct our vertically resolved MSE analysis for the simulated MJO. We will compare the results from E3SM and E3SM-MMF simulations with a focus on convective MSE transport. It is likely that traditional convection parameterizations cannot efficiently transport boundary layer high-MSE air to the free troposphere and properly distribute it, so convection's contributions to MJO's maintenance and propagation are underestimated.

7 Open Research

The E3SM project, code, simulation configurations, model output, and tools to work with the output are described on its website (`https://e3sm.org`). Instructions on how to get started with running E3SM are available on the website (`https://e3sm.org/model/running-e3sm/e3sm-quick-start`). All code for E3SM may be accessed on the GitHub repository (`https://github.com/E3SM-Project/E3SM`). The raw output data from E3SM-MMF used in this study are archived in the National Energy Research Scientific Computing Center (NERSC). The specific branch used to conduct the simulations can be found at `https://github.com/E3SM-Project/E3SM/tree/whannah/mmf/rce-with-rotation` and is also archived at `https://doi.org/10.5281/zenodo.10989362`. The analysis code and a condensed version of the data needed to reproduce our results are also archived at `https://doi.org/10.5281/zenodo.10998360`.

Acknowledgments

This work was supported by a Packard Fellowship in Science and Engineering and an NSF CAREER Award (AGS-2048268) to Da Yang. This research was supported by the Exascale Computing Project (17-SC-20-SC), a collaborative effort of the U.S. Department of Energy Office of Science and the National Nuclear Security Administration and by the Energy Exascale Earth System Model (E3SM) project, funded by the U.S. Department of Energy, Office of Science, Office of Biological and Environmental Research. This work was performed under the auspices of the U.S. Department of Energy by Lawrence Livermore National Laboratory under Contract DE-AC52-07NA27344. This research used resources of the National Energy Research Scientific Computing Center (NERSC), a U.S. Department of Energy Office of Science User Facility operated under Contract No. DE-AC02-05CH11231.

References

Adames, Á., & Kim, D. (2016). The MJO as a dispersive, convectively coupled moisture wave: theory and observations. *Journal of the Atmospheric Sciences*, *73*. doi: 10.1175/jas-d-15-0170.1

Ahmed, F. (2021). The MJO on the equatorial beta plane: An eastward-propagating rossby wave induced by meridional moisture advection. *Journal of the Atmospheric Sciences*, *78*. doi: 10.1175/JAS-D-21-0071.1

Andersen, J. A., & Kuang, Z. (2012). Moist static energy budget of MJO-like disturbances in the atmosphere of a zonally symmetric aquaplanet. *Journal of Climate*, *25*. doi: 10.1175/JCLI-D-11-00168.1

Arnold, N., & Randall, D. (2015). Global-scale convective aggregation: Implications for the Madden-Julian Oscillation. *Journal of Advances in Modeling Earth Systems*, *7*. doi: 10.1002/2015MS000498

Charney, J. (1963). A note on large-scale motions in the tropics. *Journal of the Atmospheric Sciences*, *20*. doi: 10.1175/1520-0469(1963)020⟨0607:ANOLSM⟩2.0.CO;2

Chikira, M. (2014). Eastward-propagating intraseasonal oscillation represented by chikira–sugiyama cumulus parameterization. Part II: Understanding moisture variation under weak temperature gradient balance. *Journal of the Atmospheric Sciences*, *71*. doi: 10.1175/JAS-D-13-038.1

Emanuel, K., Neelin, D., & Bretherton, C. (1994). On large-scale circulations in convecting atmospheres. *Quarterly Journal of the Royal Meteorological Society*, *120*. doi: 10.1002/qj.49712051902

Gill, A. (1980). Some simple solutions for heat-induced tropical circulation. *Quarterly Journal of the Royal Meteorological Society*, *106*. doi: 10.1002/qj.49710644905

Golaz, J., Caldwell, P. M., Van Roekel, L. P., Petersen, M. R., Tang, Q., Wolfe, J. D., ... Zhu, Q. (2019, 3). The DOE E3SM coupled model version 1: Overview and evaluation at standard resolution. *Journal of Advances in Modeling Earth Systems*, 2018MS001603. doi: 10.1029/2018MS001603

Grabowski, W. (2003). MJO-like coherent structures: Sensitivity simulations using the cloud-resolving convection parameterization (crcp). *Journal of the Atmospheric Sciences*, *60*. doi: 10.1175/1520-0469(2003)060⟨0847:MLCSSS⟩2.0.CO;2

Haertel, P., Kiladis, G., Denno, A., & Rickenbach, T. (2008). Vertical-mode decompositions of 2-day waves and the Madden–Julian Oscillation. *Journal of the Atmospheric Sciences*, *65*. doi: 10.1175/2007JAS2314.1

Hannah, W., Bradley, A. M., Guba, O., Tang, Q., Golaz, J.-C., & Wolfe, J. (2021, 7). Separating Physics and Dynamics Grids for Improved Computational Efficiency in Spectral Element Earth System Models. *Journal of Advances in Modeling Earth Systems*, *13*(7), e2020MS002419. doi: 10.1029/2020MS002419

Hannah, W., Jones, C. R., Hillman, B. R., Norman, M. R., Bader, D. C., Taylor, M. A., ... Lee, J. M. (2020, 1). Initial Results From the Super-Parameterized E3SM. *Journal of Advances in Modeling Earth Systems*, *12*(1). doi: 10.1029/2019MS001863

Hannah, W., & Pressel, K. (2022). A method for transporting cloud-resolving model variance in a multiscale modeling framework. *Geoscientific Model Development*, *15*(24), 8999–9013. doi: 10.5194/gmd-15-8999-2022

Hannah, W., Pressel, K., Ovchinnikov, M., & Elsaesser, G. (2022). Checkerboard patterns in e3smv2 and e3sm-mmfv2. *Geoscientific Model Development*, *15*(15), 6243–6257. doi: 10.5194/gmd-15-6243-2022

Holtslag, A. A. M., & Boville, B. A. (1993). Local versus nonlocal boundary-layer diffusion in a global climate model. *Journal of Climate*, *6*(10), 1825 - 1842. Retrieved from `https://journals.ametsoc.org/view/journals/clim/6/10/1520-0442_1993_006_1825_lvnbld_2_0_co_2.xml` doi: 10.1175/1520-0442(1993)006⟨1825:LVNBLD⟩2.0.CO;2

Hu, Y., Yang, D., & Yang, J. (2008). Blocking systems over an aqua planet. *Geophysical Research Letters*, *35*. doi: 10.1029/2008GL035351

Hurrell, J. W., Holland, M. M., Gent, P. R., Ghan, S., Kay, J. E., Kushner, P. J., ... Marshall, S. (2013, 9). The Community Earth System Model: A Framework for Collaborative Research. *Bulletin of the American Meteorological Society*, *94*(9), 1339–1360. doi: 10.1175/BAMS-D-12-00121.1

Khairoutdinov, M., & Emanuel, K. (2018). Intraseasonal variability in a cloud-permitting near-global equatorial aquaplanet model. *Journal of the Atmospheric Sciences*, *75*. doi: 10.1175/JAS-D-18-0152.1

Khairoutdinov, M., & Randall, D. (2003). Cloud resolving modeling of the ARM summer 1997 IOP: Model formulation, results, uncertainties, and sensitivities. *Journal of the Atmospheric Sciences*, *60*, 607–625.

Khairoutdinov, M., Randall, D. A., & DeMott, C. A. (2005). Simulations of the atmospheric general circulation using a cloud-resolving model as a superparameterization of physical processes. *Journal of the Atmospheric Sciences*, *62*, 2136–2154.

Lorenz, E. (1954). Available potential energy and the maintenance of the general circulation. *Tellus*, *7*. doi: 10.3402/tellusa.v7i2.8796

Ma, D., & Kuang, Z. (2011). Modulation of radiative heating by the Madden-Julian Oscillation and convectively coupled Kelvin waves as observed by CloudSat. *Geophysical Research Letters*, *38*. doi: 10.1029/2011GL049734

Majda, A. J., & Stechmann, S. N. (2009). The skeleton of tropical intraseasonal oscillations. *Proceedings of the National Academy of Sciences*, *106*. doi: 10.1073/pnas.0903367106

Pritchard, M., & Yang, D. (2016). Response of the superparameterized Madden–Julian Oscillation to extreme climate and basic-state variation challenges a moisture mode view. *Journal of Climate*, *29*. doi: 10.1175/JCLI-D-15-0790.1

Ronchi, C., Iacono, R., & Paolucci, P. (1996, 3). The "Cubed Sphere": A New Method for the Solution of Partial Differential Equations in Spherical Geometry. *Journal of Computational Physics*, *124*(1), 93–114. doi: 10.1006/JCPH.1996.0047

Seidel, S., & Yang, D. (2020). The lightness of water vapor helps to stabilize tropical climate. *Science Advances*, *6*. doi: 10.1126/sciadv.aba1951

Straub, G. K. K., & Haertel, P. (2005). Zonal and vertical structure of the Madden–Julian Oscillation. *Journal of the Atmospheric Sciences*, *62*. doi: 10.1175/JAS3520.1

Taylor, M. A., Edwards, J., Thomas, S., & Nair, R. (2007, 7). A mass and energy conserving spectral element atmospheric dynamical core on the cubed-sphere grid. *Journal of Physics: Conference Series*, *78*(1), 012074. doi: 10.1088/1742-6596/78/1/012074

Wang, B., & Chen, J. (1989). On the zonal-scale selection and vertical structure of equatorial intraseasonal waves. *Quarterly Journal of the Royal Meteorological Society*, *115*. doi: 10.1002/qj.49711549007

Wang, B., Lee, S.-S., Waliser, D., Zhang, C., Sobel, A., Maloney, E., ... Ha, K.-J. (2018). Dynamics-oriented diagnostics for the Madden–Julian Oscillation. *Journal of Climate*, *31*. doi: 10.1175/JCLI-D-17-0332.1

Wang, B., Liu, F., & Chen, G. (2016). A trio-interaction theory for Madden–Julian Oscillation. *Geoscience Letters*, *3*. doi: 10.1186/s40562-016-0066-z

Wang, B., & Rui, H. (1990). Dynamics of the coupled moist Kelvin–Rossby wave on an equatorial β-plane. *Journal of the Atmospheric Sciences*, *47*. doi: 10.1175/1520

-0469(1990)047⟨0397:DOTCMK⟩2.0.CO;2
Wheeler, M., & Kiladis, G. (1999). Convectively coupled equatorial waves: Analysis of clouds and temperature in the wavenumber–frequency domain. *Journal of the Atmospheric Sciences*, *56*. doi: 10.1175/1520-0469(1999)056⟨0374:CCEWAO⟩2.0.CO;2
Wing, A. A., Reed, K. A., Satoh, M., Stevens, B., Bony, S., & Ohno, T. (2018). Radiative–convective equilibrium model intercomparison project. *Geoscientific Model Development*, *11*(2), 793–813. doi: 10.5194/gmd-11-793-2018
Wolding, B., Maloney, E., & Branson, M. (2016). Vertically resolved weak temperature gradient analysis of the Madden-Julian Oscillation in SP-CESM. *Journal of Advances in Modeling Earth Systems*, *8*. doi: 10.1002/2016MS000724
Xie, S., Lin, W., Rasch, P. J., Ma, P.-L., Neale, R., Larson, V. E., ... Zhang, Y. (2018, 10). Understanding Cloud and Convective Characteristics in Version 1 of the E3SM Atmosphere Model. *Journal of Advances in Modeling Earth Systems*, *10*(10), 2618–2644. doi: 10.1029/2018MS001350
Yang, D. (2018a). Boundary layer diabatic processes, the virtual effect, and convective self-aggregation. *Journal of Advances in Modeling Earth Systems*, *10*. doi: 10.1029/2017MS001261
Yang, D. (2018b). Boundary layer height and buoyancy determine the horizontal scale of convective self-aggregation. *Journal of the Atmospheric Sciences*, *75*. doi: 10.1175/JAS-D-17-0150.1
Yang, D., & Ingersoll, A. P. (2013). Triggered convection, gravity waves, and the MJO: A shallow-water model. *Journal of the Atmospheric Sciences*, *70*. doi: 10.1175/jas-d-12-0255.1
Yang, D., & Ingersoll, A. P. (2014). A theory of the MJO horizontal scale. *Geophysical Research Letters*, *41*. doi: 10.1002/2013GL058542
Yang, D., & Seidel, S. D. (2020). The incredible lightness of water vapor. *Journal of Climate*, *33*. doi: 10.1175/JCLI-D-19-0260.1
Yang, D., Zhou, W., & Seidel, S. (2022). Substantial influence of vapour buoyancy on tropospheric air temperature and subtropical cloud. *Nature Geoscience*, *15*. doi: 10.1038/s41561-022-01033-x
Yao, L., & Yang, D. (2023). Convective self-aggregation occurs without radiative feedbacks in warm climates. *Geophysical Research Letters*, *50*. doi: 10.1029/2023GL104624
Yao, L., Yang, D., & Tan, Z.-M. (2022). A vertically resolved MSE framework highlights the role of the boundary layer in convective self-aggregation. *Journal of the Atmospheric Sciences*, *79*, 1615–1631. doi: 10.1175/JAS-D-20-0254.1
Zhang, B., Soden, B., & Vecchi, G. (2022). A vertically resolved analysis of radiative feedbacks on moist static energy variance in tropical cyclones. *Journal of Climate*, *36*. doi: 10.1175/JCLI-D-22-0199.1
Zhang, C. (2005). Madden-Julian Oscillation. *Reviews of Geophysics*, *43*. doi: 10.1029/2004RG000158
Zhang, C., Adames, Á., Khouider, B., Wang, B., & Yang, D. (2020). Four theories of the Madden-Julian Oscillation. *Reviews of Geophysics*, *58*. doi: 10.1029/2019RG000685

Supporting Information for "Vertically resolved analysis of the Madden-Julian Oscillation highlights the role of convective transport of moist static energy"

Da Yang[1], Lin Yao[1], and Walter Hannah[2]

[1]Department of the Geophysical Sciences, University of Chicago, Chicago, IL, USA

[2]Atmospheric, Earth and Energy Division, Lawrence Livermore National Laboratory, Livermore, CA, USA

Contents of this file

Text S1. Horizontal Structures of the MJO composite

Figure S1 shows that the MJO composites in the control and the mechanism-denial experiments share similar horizontal structures.

Text S2. Vertical Structures of the MJO composite

Figure S2 shows the vertical structures of the MJO composite in the control experiment. The results complement Figure 3 by showing the combined contribution of convection

---

(CRM), boundary layer, and large-scale dynamics to the tendencies of DSE and moisture components.

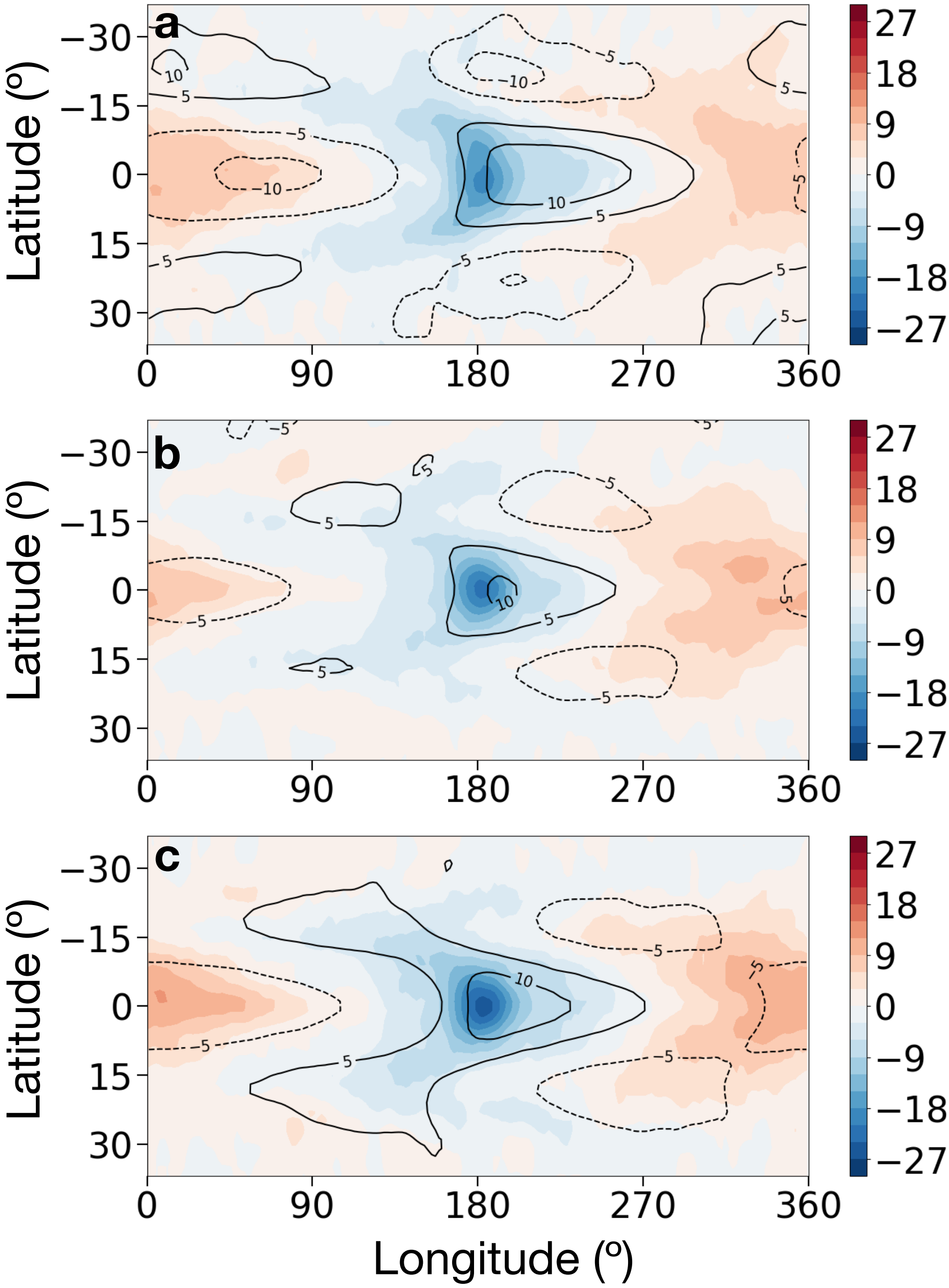

Figure S1. Horizontal structure of the MJO composite. (a) The control simulation. (b) The HomoRad simulation. (c) The FixedRad simulation. Color shading represents OLR anomalies, and contours represent geopotential anomalies associated with the MJO.

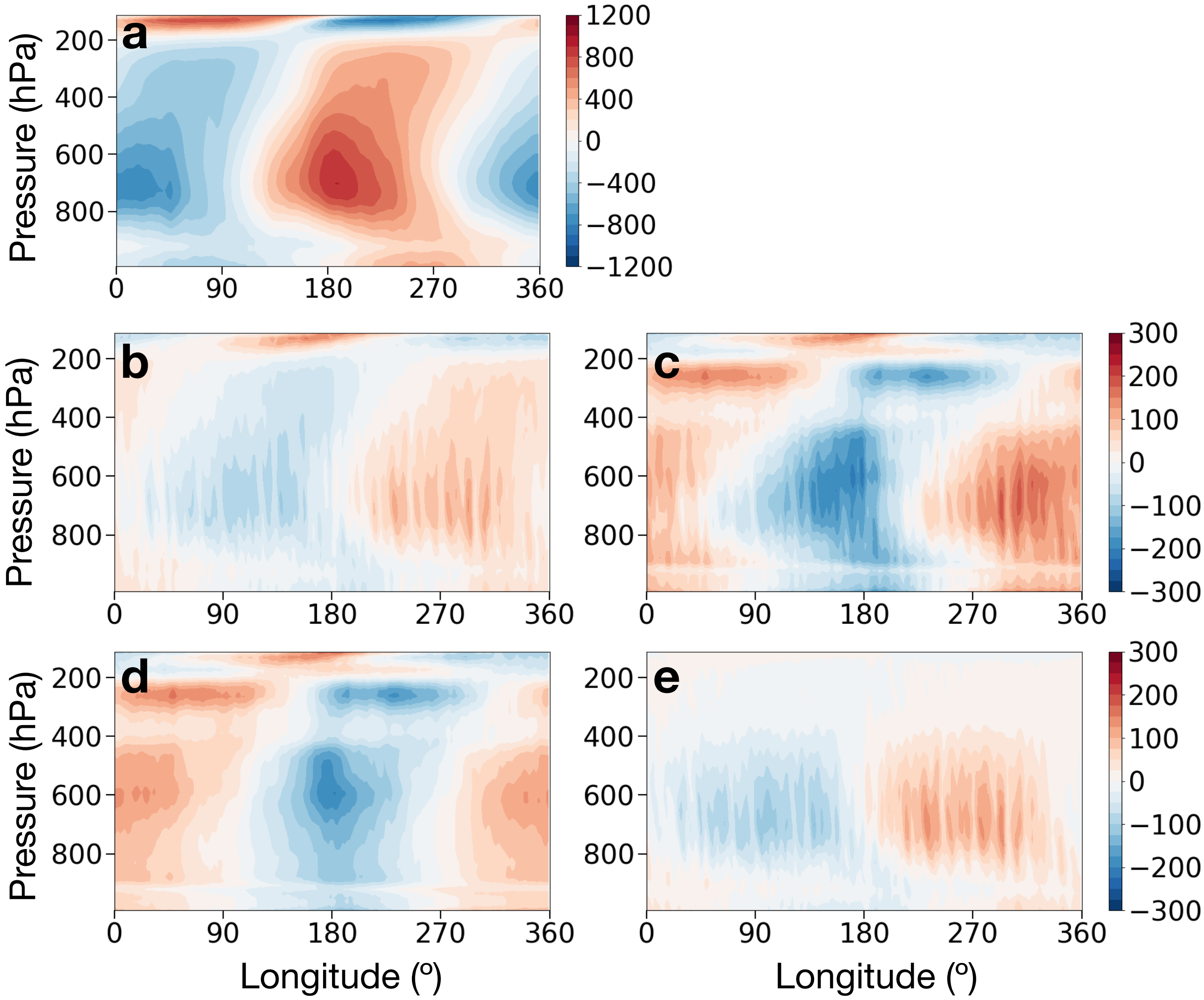

Figure S2. Vertical structures of the MSE budget of the MJO composite. (a) The MJO's MSE anomaly (J/kg). (b) Total MSE tendency ∂_tMSE (J/kg/day). (c) Total MSE tendency due to convection (CRM), boundary layer, and large-scale dynamics (J/kg/day). (d) and (e) show the DSE and moisture components of (c), respectively (J/kg/day).